**Article:**
Kouroussis, G, Vogiatzis, KE and Connolly, DP (2018) Assessment of railway ground vibration in urban area using in-situ transfer mobilities and simulated vehicle-track interaction. International Journal of Rail Transportation, 6 (2). pp. 113-130. ISSN: 2324-8378

https://doi.org/10.1080/23248378.2017.1399093

# Assessment of railway ground vibration in urban area using in-situ transfer mobilities and simulated vehicle-track interaction

**Georges Kouroussis[1], Konstantinos E. Vogiatzis[2] and David P. Connolly[3]**

[1.] *University of Mons, Faculty of Engineering, Department of Theoretical Mechanics, Dynamics and Vibrations, Place du Parc 20, 7000 Mons, Belgium*

[2.] *University of Thessaly, Department of Civil Engineering, Laboratory of Transportation Environmental Acoustics, Pedion Areos, Volos 383 34, Greece*

[3.] *University of Leeds, Institute for High Speed Rail Engineering, Leeds, LS2 9JT, United Kingdom*

**Abstract:** This paper proposes an alternative approach to the well-known Federal Railroad Administration (2012) method to evaluate ground vibrations induced by the passing of railway vehicles. The originality lies on the excitation mechanisms that occur in urban areas. A common source of railway-induced ground vibrations is local defects (rail joints, switches and turnouts) which cause large amplitude excitations at isolated locations along the track. To analyse such situations, a combined numerical-experimental study is developed, based on the use of numerical train/track results and experimental mobility transfer functions. The influence of building type, vehicle, defect type and size and location is evaluated through experimental data collected in Brussels (Belgium). The results show that it is possible to assess vibrations from light rapid transit systems in the presence of local rail defects and unknown soil conditions.

**Keywords:** ground vibration; impact force; measurement on building; turnout; rail joint; Brussels tram

## 1 Introduction

Modern tram and metro networks represent an interesting modal shift by improving the quality of life of people by significantly alleviating traffic congestion and pollution, especially in urban areas. A potential challenge of tram networks is the exposure of residents to railway vibrations. Considerable efforts have been made in order to reduce the generated vibrations in many areas, from designing mitigation solutions (e.g. on the vehicle (Nielsen et al., 2015), at the wheel/rail interface (Talbot, 2014), on the track (Zhu et al., 2017a, 2015b), on the trackbed (Vogiatzis, 2015) and at the receiver (Talbot, 2016)).. Local defects, especially turnouts and rail joints, when designed poorly, are often the origin of high levels of vibration. As discussed in Connolly et al. (2016), the majority of actions are preferred at the track structure (active mitigation), rather than the implementation of a more passive solution in the far-field.

Predicting ground-borne vibrations in existing and new situations is challenging due to the lack of site information, especially regarding the soil configuration. In such cases, the use of dynamic transfer functions to characterize the track/soil subsystem offers a rapid way to evaluate soil amplification factors. The technique developed by Nelson and Saurenman (1987) for predicting ground borne noise and vibration from railway vehicles uses this approach. This technique is often called the "FRA2012 method" since the Federal Railroad Administration of the U.S. Department of Transportation (2012) adopted it for assessing the impact of railway ground vibration. The main focus of this tool is to estimate the ground-borne noise and vibration between 6.3 - 200 Hz in residential areas near at-grade and subway tracks. The problem is reduced to estimating ground surface vibration with the help of the line transfer mobility, defined as a function of the frequency $f$,

$$M_{L,i} = 10\log_{10}\left(d\sum_{j=1}^{l} M_{i,j}\right) \quad (1)$$

where $d$ is the distance between each source considered and $M_{i,j}$ is one of the $l$ point source transfer mobilities between points $i$ and $j$ (Figure 1). The line transfer mobility is often defined using decibel scales. The force density $L_F$ can be obtained from tests (as suggested by Federal Railroad Administration of the U.S. Department of Transportation (2012)) or using numerical data, as proposed by Verbraken et al. (2011). The resulting vibration is calculated at distance $y_i$ from the track to predict the vibration velocity level

$$L_{V,i} = L_F + M_{L,i} \ . \quad (2)$$

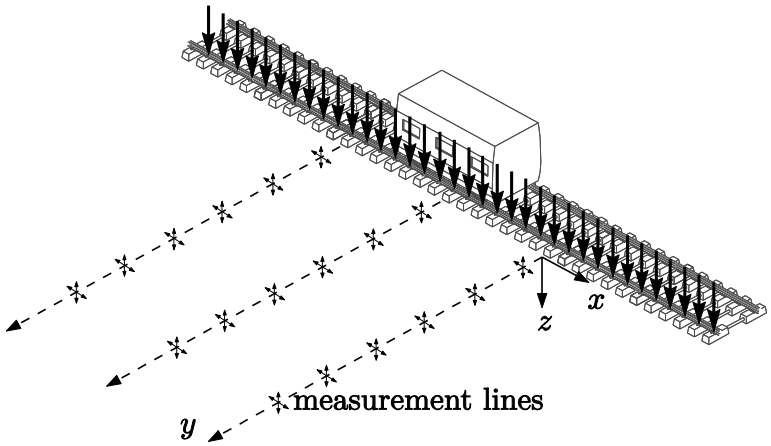


**Fig. 1 Setup for vibration propagation tests for distributed sources (line transfer excitation)**

It must be noted that the FRA2012 approach is based on the frequency domain analysis (no information about vibration phase available) and rms-like indicators (velocity decibels) can be derived for a quantitative analysis. A recent analysis also showed that physical transfer function tests were used on 85% of technical ground-borne vibration impact assessment studies (Connolly et al., 2016), as illustrated in Figure 2. This demonstrates the common acceptance of in-situ drop-weight experiments to characterize the vibration responses of track, soil and buildings.

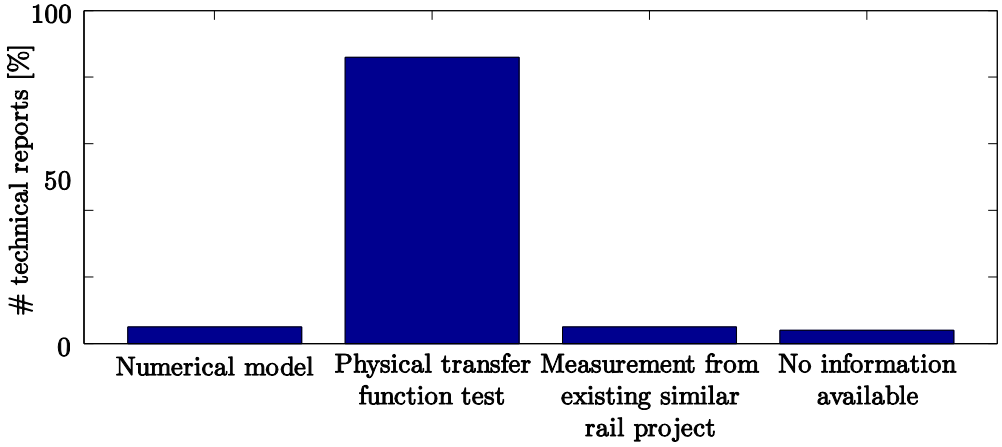


**Fig. 2 Vibration prediction approaches used in 56 commercial ground-borne noise and vibration reports analysed in Connolly et al., (2016)**

Alternative scoping approaches are available using neural network approaches coupled with numerical models that predict vibration levels in terms of velocity decibels, in the presence of multi-layered soils (Connolly, Kouroussis, Giannopoulos, Verlinden, Woodward and Forde, 2014; Connolly, Kouroussis, Woodward, Verlinden, Giannopoulos and Forde, 2014),. Auersch (2015) also presented a backward

analysis to calculate the axle-load spectra from measured ground vibration spectra and transfer mobility data. Paneiro et al. (2016) developed quantitative and qualitative predictors based on a neural network approach dedicated to light railway traffic in urban areas.
These aforementioned methods give results only when a distributed excitation source is considered and local excitations are neglected (e.g. high-speed lines). The situation is significantly different in the case of urban transit, due to the presence of local defects which induce elevated and localised vibrations (Kouroussis et al., 2015a, 2015b). The use of line-source transfer mobilities is thus not suitable for the present case as the assumption of track invariability is no longer valid. The objective of this paper is to show that source transfer mobility functions can be used to assess the vibration levels generated by local defects. A hybrid numerical/experimental prediction model is described and presented with an illustrative case from Brussels, focusing on the effect of local defects at various locations inside the Brussels region.

## 2 Hybrid numerical/experimental prediction model

### *2.1 Step 1: Predicting the wheel/rail forces using a vehicle/track/foundation model*

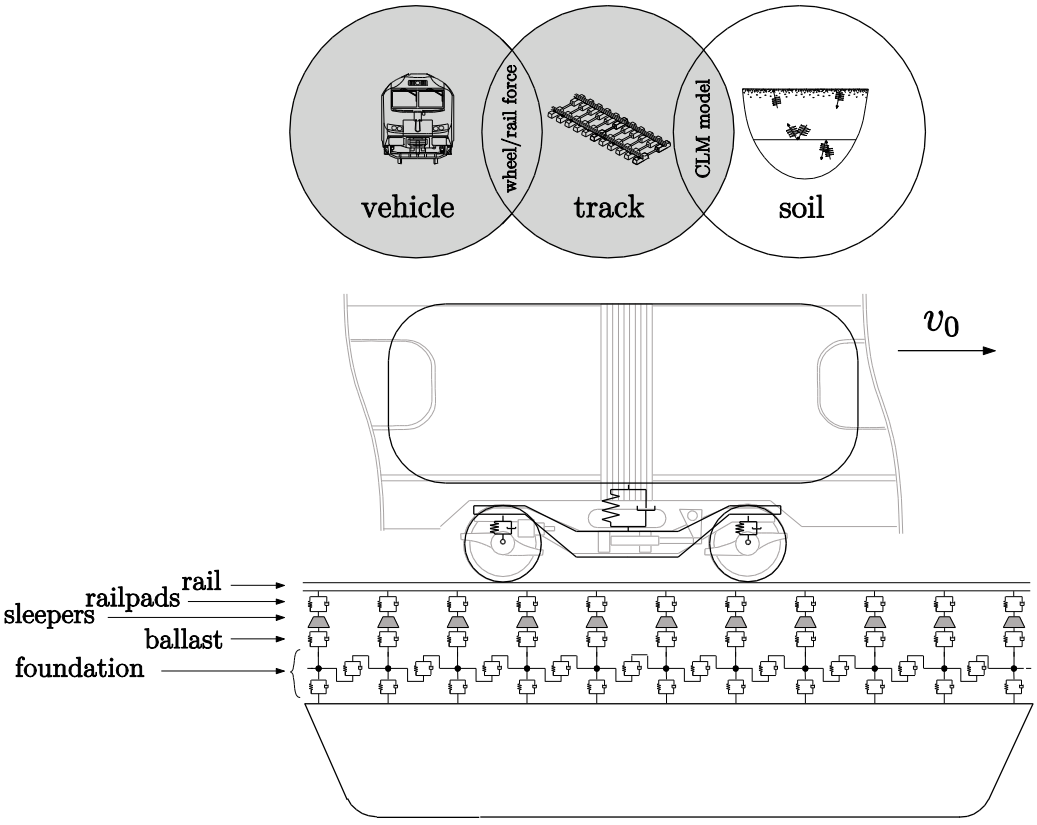


**Fig. 3 Vehicle/track/foundation simulation model (Olivier et al., 2016)**

The proposed vehicle/track/foundation prediction methodology is summarized in Figure 3. Derived from the model of Zhai and Sun (1994), it consists of a classical multibody approach for the vehicle coupled with a finite element/lumped mass model for the track. The latter model lies on the foundation represented by a coupled lumped mass (CLM) model. The system is described by its mass, damping, and stiffness matrices built from its mechanical and geometrical properties. This offers a way to accurately predict the track response at low frequencies where the foundation plays an important role, thus requiring accurate track-soilcoupling (Kouroussis and Verlinden, 2015).

The track is defined as a rail modelled by a Euler–Bernoulli beam, and discretely supported sleepers. The degrees of freedom of the vehicle are in the same plane as the track. The flexible rail is modelled with the finite element method. The sleepers have a lumped mass, and a constant spacing between each sleeper. Viscoelastic properties are considered for the railpads and ballast, which is characterised by springs and dampers. The wheel/rail contact forces are defined to couple both the vehicle and track subsystems, explicitly considered as non-linear and dependent on the wheel position and its contact with the rail

$$F_{wheel/rail,i} = K_{Hz}(z_{wheel,i} - z_{rail}(x_j) - h_{defect})^{3/2} \quad . \qquad (3)$$

This connection force depends on the vertical position $z_{wheel,i}$ of the wheel and the corresponding vertical displacement $z_{rail}(x_j)$ of the rail at coordinate $x_j$. $K_{Hz}$ is the Hertz's coefficient (in N/m$^{2/3}$). The vertical dynamic response of the vehicle/track subsystem due to the rail irregularity $h_{defect}$ is therefore calculated, including the geometry of the studied local defect (represented by an analytical function) and the wheel curvature. Figure 4 displays some defect shapes studied in the present research works taking in to account the wheel radius of the wheelset and as a function of their height *h* and their length *l*.

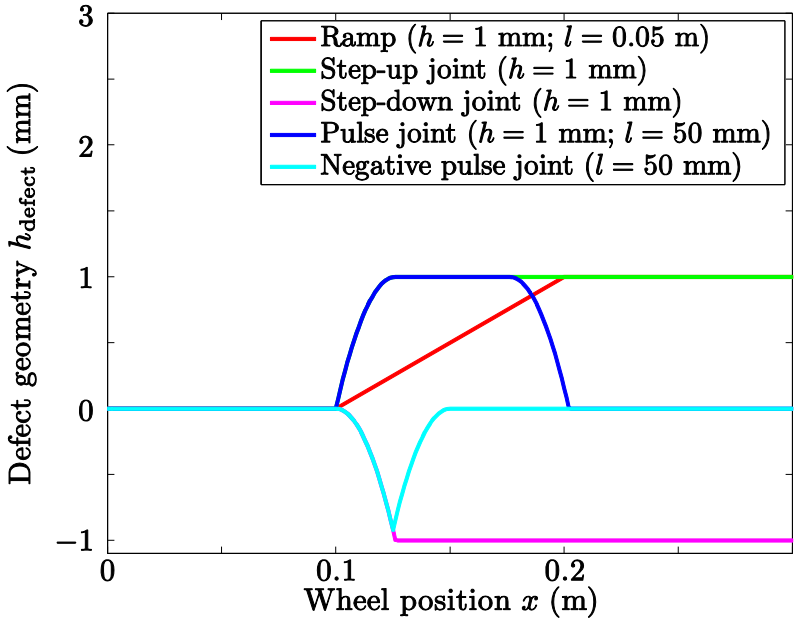


**Fig. 4 Quantitative comparison of the studied defects, with a wheel radius of 340 mm**

The simulation of the vehicle/track/foundation system is made in the time domain for a vehicle speed $v_0$ (assumed to be constant in the present work), with the help of an in-house C++ library called EasyDyn (Verlinden et al., 2013). As an alternative to a Winkler foundation, a CLM model has been developed for the track/soil coupling (Kouroussis et al., 2011).This model takes into account the coupling between foundations, representing the contact soil area supporting the sleeper through the ballast.

The wheel/rail contact forces $F_{wheel/rail,i}$ acting on the defect location are saved during the simulation. These forces are used to define the force density $L_F$ to characterize the excitation forces generated by the interaction of the vehicle with the local defect.

### *2.2 Step 2: Soil mobility transfer estimation*

The basis of this method is the measurement of a single source transfer mobility function between various points *i* on a system. This function gives the dynamic transfer characteristics between two points of the system — the soil velocity response $X_i$ and the force $F_j$ acting at the soil surface —

and yields soil dynamic information in the frequency domain (Bovey, 1983). A single source transfer mobility is theoretically defined as

$$M_{i,j} = \frac{X_i}{F_j} \ . \tag{4}$$

Regarding the aforementioned railway-induced ground vibration problem, as the number of point transfer mobilities increases, the higher the accuracy of the calculation Eq. (1) in assessing the problem of distributed irregularities along the track and/or the effects of a high-speed train. However, if the study is focused on low speeds and the dynamic effects of local defects, one-point transfer mobility remains sufficient to evaluate the vibratory effects of ground wave propagation. This second case is highly applicable to urban environments (Figure 5).

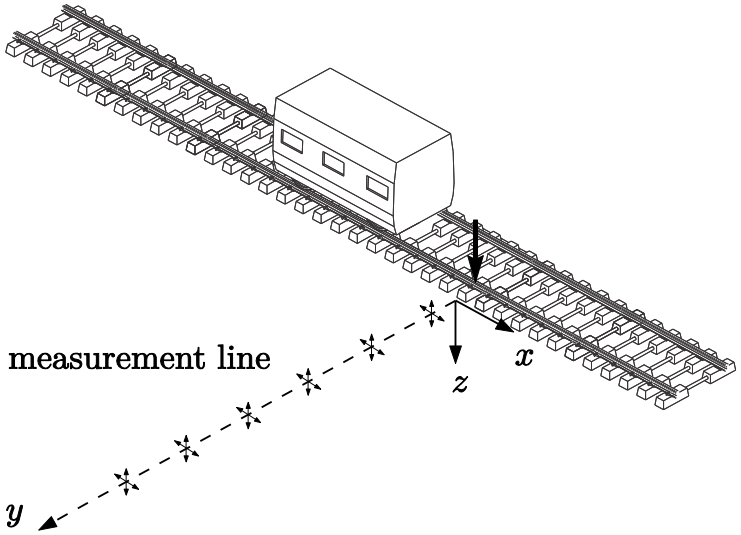


**Fig. 5 Setup for vibration propagation tests for local sources of excitation.**

In order to generate the transfer mobility function $M_{i,j}$ between two points *i* and *j*, simultaneous analyses must be performed on data signals representing the input force applied at point *i* of the system (usually by performing an impulse load/impact force) and the system response measured at a different point *j*

$$M_{i,j} = \frac{S_{F_j X_i(f)}}{S_{F_j F_j(f)}} \tag{5}$$

where auto-spectrum of the excitation $S_{F_j F_j(f)}$ and cross-spectrum of excitation and response $S_{F_j X_i(f)}$ are defined as

$$S_{F_j F_j(f)} = \frac{1}{n} \sum_{k=1}^{n} F_j^*(f) F_j(f) \tag{6}$$

$$S_{F_j X_i(f)} = \frac{1}{n} \sum_{k=1}^{n} F_j^*(f) X_i(f) \ . \tag{7}$$

In addition, the causal and linear relationship between the output and input can be physically described using the coherence function, defined as

$$\gamma^2 = \frac{\left| S_{F_j X_i(f)} \right|^2}{S_{F_j F_j(f)} \, S_{X_i X_i(f)}} \tag{8}$$

where the auto-spectrum of the response is defined as

$$S_{X_iX_i(f)} = \frac{1}{n}\sum_{k=1}^{n} X_i^*(f)X_i(f) \ . \quad (9)$$

Careful consideration needs to be given to noise and leakage when using the Fourier transform. Poor coherence is indicative of a low signal-to-noise ratio, measurement errors, non-linearity or time-variant behaviour of the structure, or a combination of the aforementioned factors. Depending on the type of measurement used to detect the response motion, the soil velocity response $X_i(f)$ may be calculated as one derivative or one integration. Robust signal processing techniques are therefore required to avoid non-physical signals associated with the integration constant or the derivative gradient inherent to the original noisy signal and the sampling rate.
Several accelerometers or geophones can be placed along a profile perpendicular to the track, and used to measure the vertical soil response (Figure 6). The distance from the track is identified from the edge of the closest rail. A first accelerometer could be placed close to the track (tram site edge) and the other at distant points of interest (e.g. near sensitive buildings, foundation walls of dwellings, etc.). If the number of sensors is sufficient, the attenuation of ground vibrations with distance can be calculated, as well as the decay of the frequency content (soil filtering) and the scattering effect of the soil heterogeneity.

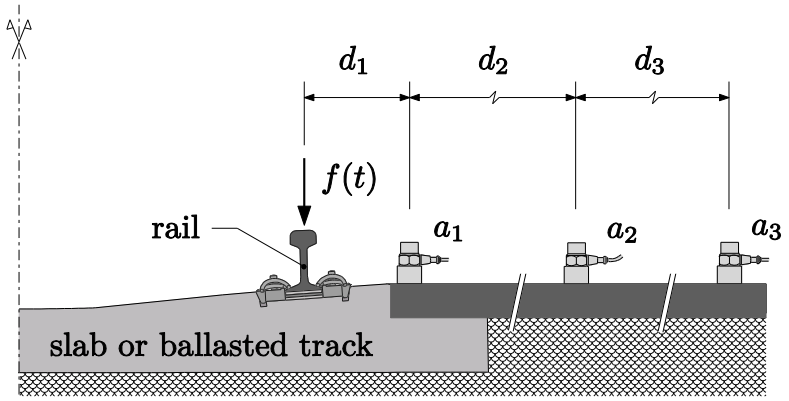


**Fig. 6 Experimental setup and location of the sensors**

The impact force may be applied to the structure by various methods. One common way to excite structures is through the use of a sledge/impact hammer. A dynamic impulse hammer with an embedded force sensor is an efficient exciter, easy to use and very portable. It must, however, excite the structure with constant force over the frequency range of interest. Moreover, the weight of the hammer and the number of impacts impose physical requirements from the operator and a reliable series of impacts are not always necessarily obtained (Bovey, 1983). This is why a mechanical exciter in the form of a drop hammer impactor was used as an alternative. In the present work, a falling mass machine was used to perform the tests. It consists of a steel frame serving as a guidance support for a falling mass. The latter is constituted by several heavy masses (12.5 kg each) and an elastomer support to allow for the filtering to the desired frequency range. The total mass can be up to 52 kg and be launched from a maximum height of 1.5 m. A mechanical winch is used with a handle to easily raise the mass and a seat-belt buckle serves as actuator. An accelerometer is placed on top of the mass to measure the mass acceleration (and the excitation force by multiplying the measured acceleration by the mass). A short analytical calculation proved that, for a nominal height of 1 m, the expected duration of the impact is 2.2 ms with a maximum acceleration of 200 g (corresponding to a maximum force of 10 tonnes), covering a frequency range up to 100 Hz.
Finally, the wheel/rail forces defined by Eq. (3) are saved during the first calculation step and combined with the mobility transfer function obtained from Eq. (5). Practically, the discrete Fourier transform is used to obtain the corresponding force spectra $F_{wheel}(f)$ (from all the forces $F_{wheel/rail,i}$ for each wheelset). The vibration level is thus obtained by multiplying these two parameters

$$V(f) = F_{wheel}(f)\, M_{i,j}(f) \tag{9}$$

or, using a decibel scale,

$$L_V = L_F + M_{S,i} \ . \tag{10}$$

An inverse discrete Fourier transform is then used to obtain the equivalent time histories.

# 3 Results

Experimental data from a total of 14 test locations, designated site 1 - 14, across the Brussels Region, were examined. The sites consisted of a combination of slab and ballasted tracks. The T2006 tram is used as a reference. Site choices were motivated by several complaints arising from this type of tram circulating in Brussels. No tram pass-by was recorded (due to the lack of availability of such a tram for all the studied sites) and instead only impact tests were performed (experimentally). Table 1 summarizes the various sites tested, including different track types. Special attention was paid to analyse the most common track and trackbed systems, with both concrete and wooden sleepers, and different track forms, including floating slabs (FS). Table 1 also indicates the building distances from the track, which cover distance of 2.7 to 13 m. For each site, the vibration sensor was placed at the building foundation. Where possible, sites were selected with the goal of maintaining a similar distance between the track and building.

**Tab. 1 The 14 sites tested in Brussels Region**

| **site #** | 1 | 2 | 3 | 4 | 5 | 6 | 7 | 8 | 9 | 10 | 11 | 12 | 13 | 14 |
|---|---|---|---|---|---|---|---|---|---|---|---|---|---|---|
| **type** | ballasted track | | | | | | slab track | | | | | | | |
| **subtrack** | concrete sleepers | | wood sleepers | | | | resilient material | | FS | concrete slab track | | | | |
| **Distance from the track** [m] | 13 | 2.7 | 8 | 5.3 | 7.8 | 6.9 | 11 | 4.8 | 8.7 | 7.9 | 7.9 | 7.9 | 7.9 | 7.9 |

Figures 7 and 8 present some examples of calculated wheel/rail forces obtained from the vehicle/track/foundation model. The passing of the tram T2006 at a constant speed of $v_0$ = 30 km/h over a rail joint (geometrical shape of a pulse) is shown. Both positive and negative pulse joint forces are presented. The impact of each wheel is clearly visible: each axle crosses the defect at times, $t$ = 0.98 s, $t$ = 1.19 s, $t$ = 1.89 s, $t$ = 2.09 s, $t$ = 2.79 s and $t$ = 2.99 s, with strong oscillations produced after each impact. This corresponds to a signal frequency around 16 Hz and is associated to the vehicle's bogie bounce mode.

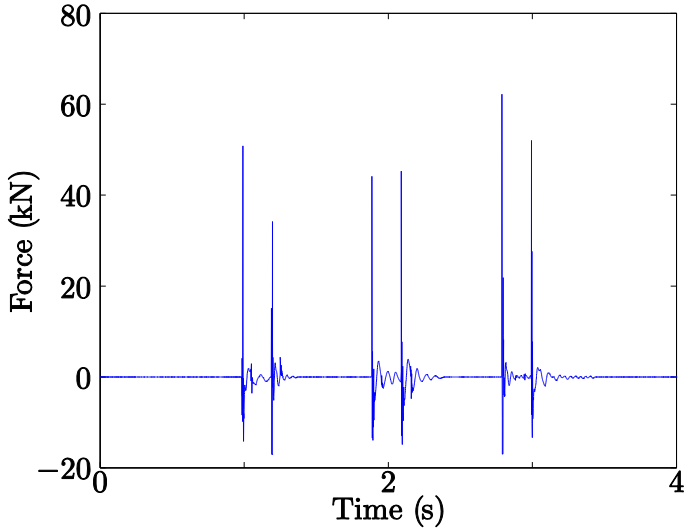


**Fig. 7 Calculated wheel/rail forces acting on defect location for a tram T2006 running at 30 km/h on a rail joint (positive pulse of height 1 mm; length 5 mm)**

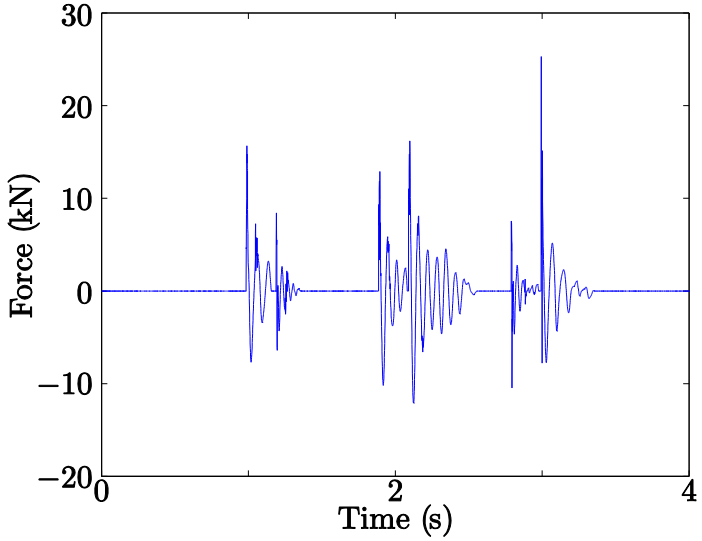


**Fig. 8 Calculated wheel/rail forces acting on defect location for a tram T2006 running at 30 km/h on a rail joint (negative pulse of length 5 mm)**

Figures 9 to 11 present some example transfer mobility function measurements (for site 1, a ballasted track with concrete sleepers; for site 6, a ballasted track with azobe sleepers and for site 12, a concrete slab track). Coherence curves are also plotted in order to define the frequency range free from measurement errors (typically between 10 - 90 Hz). Dynamic excitation generated within the track is both filtered and dampened by the soil as it propagates. This shows an attenuation with distance for the frequency range of concern: between track and building foundations, a difference of almost 10-15 dB is observable. In addition, no notable difference between ballasted tracks, including concrete or wood sleepers, were found. A mean attenuation was also approximately 15 dB. It also appears that slab tracks generally present a better vibration isolation than classic ballasted tracks. In a general way, the dynamic excitation generated within the track is both filtered and dampened by the soil as it propagates. This shows an attenuation with the distance over the entire frequency range because between the track and building foundations, a difference of approximately 10-15dB is observable. Due to the limited number of measurement locations, a more affective evaluation of this attenuation was difficult to estimate. Similar trends were also found for the alternative sites.

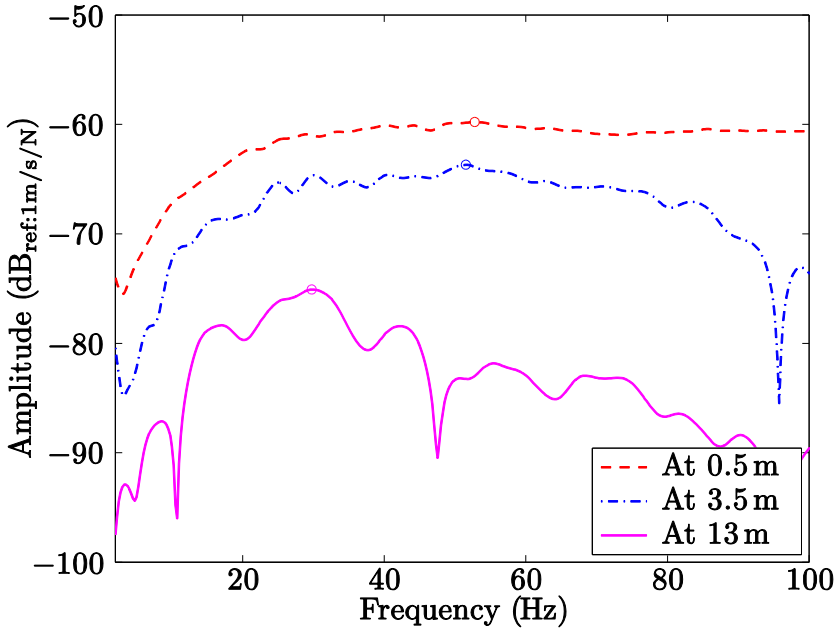


(a)

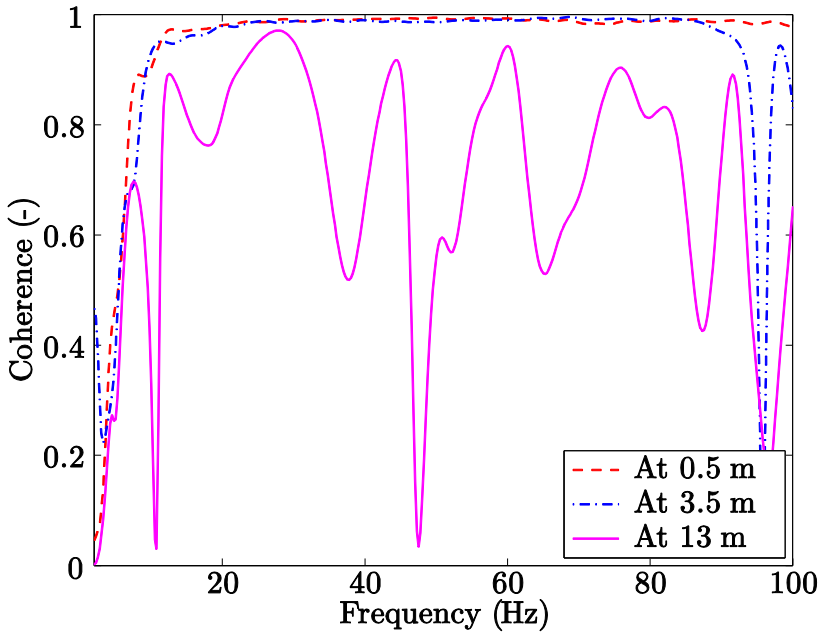


(b)

**Fig. 9 Transfer mobility functions $M_{i,j}$ for site 1 (ballasted track and concrete sleepers): (a) magnitude and (b) coherence**

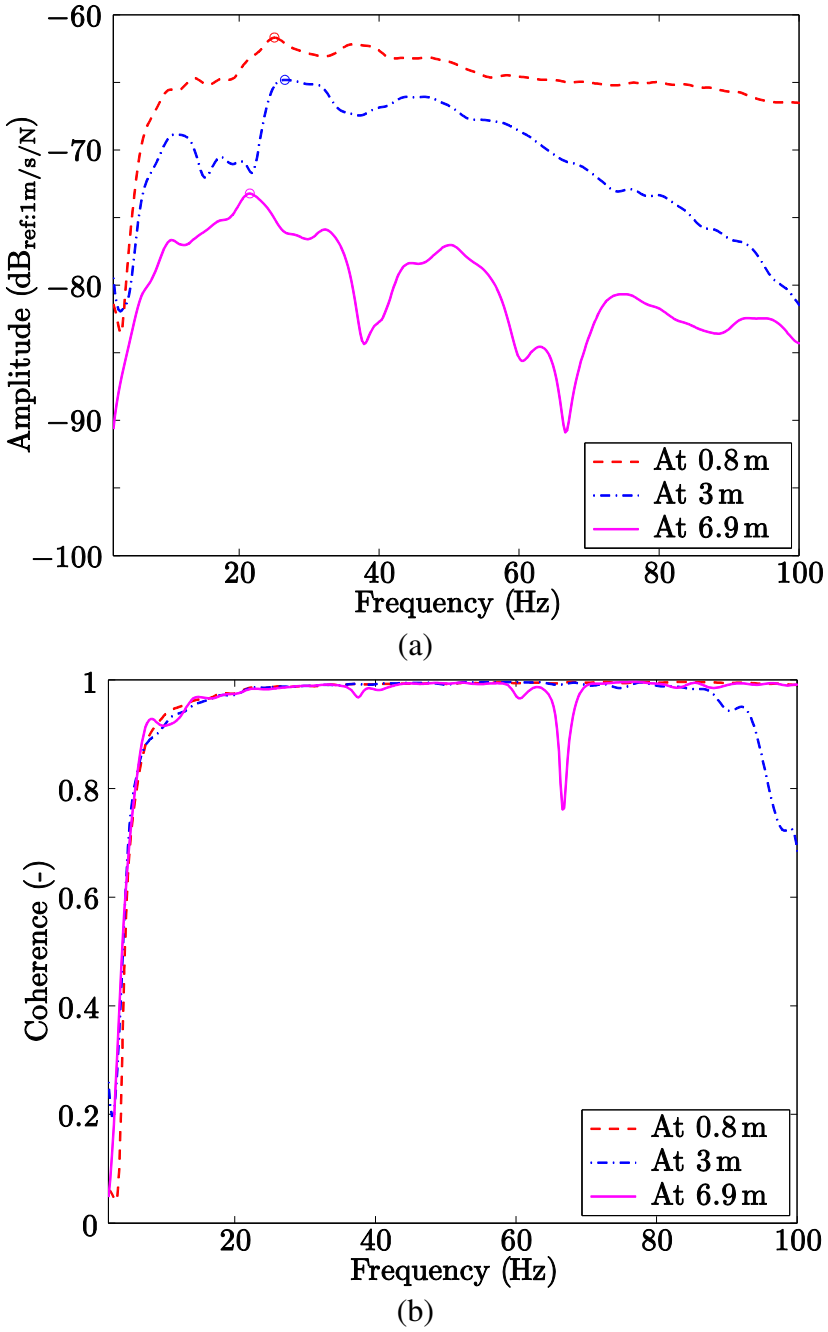


**Fig. 10 Transfer mobility functions $M_{i,j}$ for site 6 (ballasted track and azobe sleepers): (a) magnitude and (b) coherence**

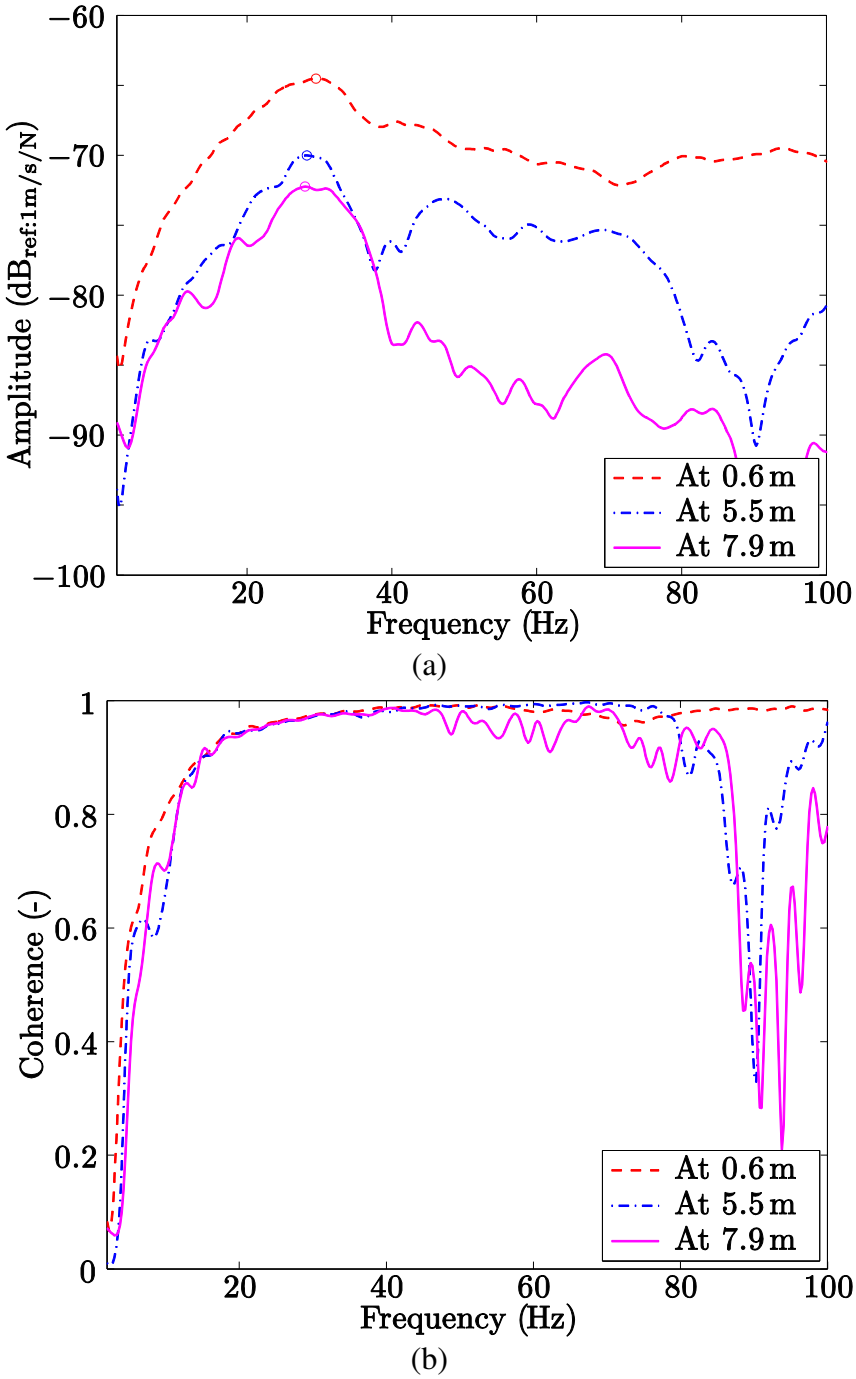


**Fig. 11 Transfer mobility functions $M_{i,j}$ for site 12 (slab track and concrete sleepers): (a) magnitude and (b) coherence**

Figure 12 shows the ground vibration results for site 12 when the tram travels over a rail joint. The response was calculated at various distances where the experimental mobility $\boldsymbol{M_{i,j}(f)}$ exists. It appears that each passing over a specific defect generates different vibration (both in shape and level). As expected, the level diminishes with distance. Figure 13 displays the corresponding frequency content of these results and reveals that the magnitude is important in the frequency range 10-30 Hz. These peaks are close to the track/soil resonance observed in Figure 11 and to the main natural frequencies of the vehicle.Previously the same tram had been the subject of a comparative analysis between the effect of the vehicle dynamics and wheel/rail forces, revealing that the bogie bounce and pitch modes play an important role, and the vibrations of the soil were essentially dominated by these natural modes (Kouroussis et al., 2013). A single peak is also visible at the very low frequency (around 2 Hz), corresponding to the car bounce mode. The dominant frequencies expected from carriage periodicity are not visible, mainly due to the absence of quasi-static effects and the low vehicle speed

(Kouroussis et al. 2014).
Figure 14 compares the peak particle velocity (*PPV*) values calculated for each experimental site, for all the studied distances. In general it appears that slab tracks (sites 7 to 14) present better vibration isolation compared to classic ballasted tracks (sites 1 to 6). Other findings observed from the site results reveal that:

- The mean foundation vibration level varies with the site. The maximum level does not exceed 5 mm/s, which usually represents a threshold for such buildings. Sites 9, 7 and 3 were found, in that order, to produce the highest *PPV*. Site 1 (with the higher track-foundation distance) does not present elevated vibration levels.
- No notable difference between ballasted tracks, including concrete (sites 1 and 2) or wood sleepers (sites 3 to 6), were found.
- The only site with a floating slab (FS), site 9, produced very high-level vibration. However, only two measurement points were used and, at this stage, it is difficult to draw significant outcomes.
- Regarding slab track sites 10 to 14 (same track-foundation distance of 7.9 m), the vibration level is relatively close between them, with the exception of site 10.

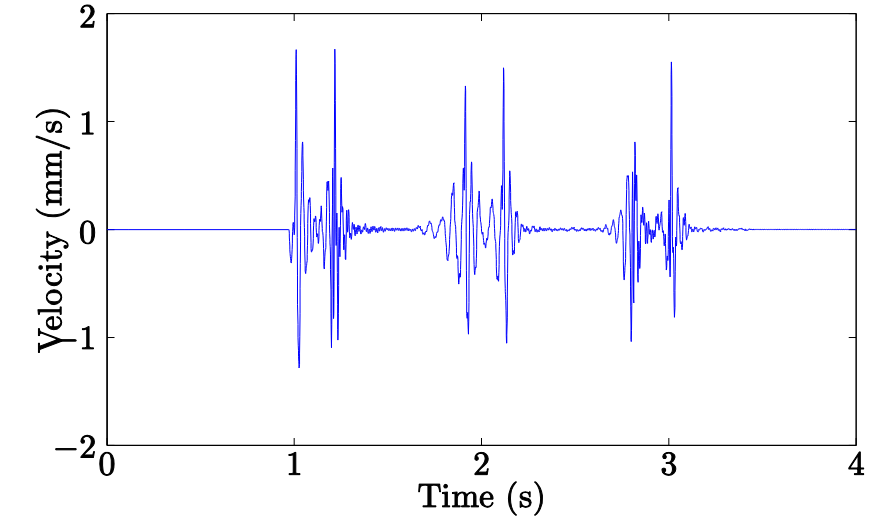

(a)

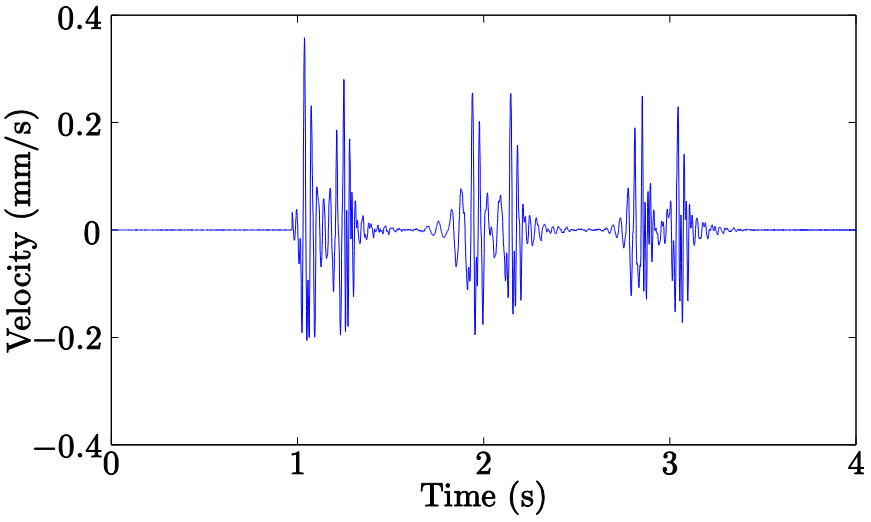

(b)

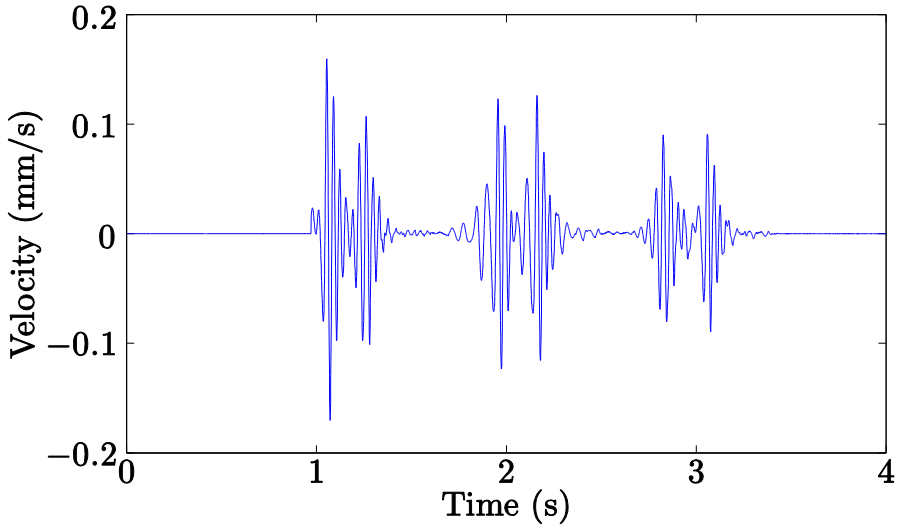


(c)

**Fig. 12 Time histories of vibration velocities predicted at various distances from the track (site 12) for a tram T2006 running at 30 km/h on a rail joint (height 1 mm; length 5 mm): (a) at 0.6 m from the track, (b) at 5.5 m from the track and (c) at 7.9 m from the track**

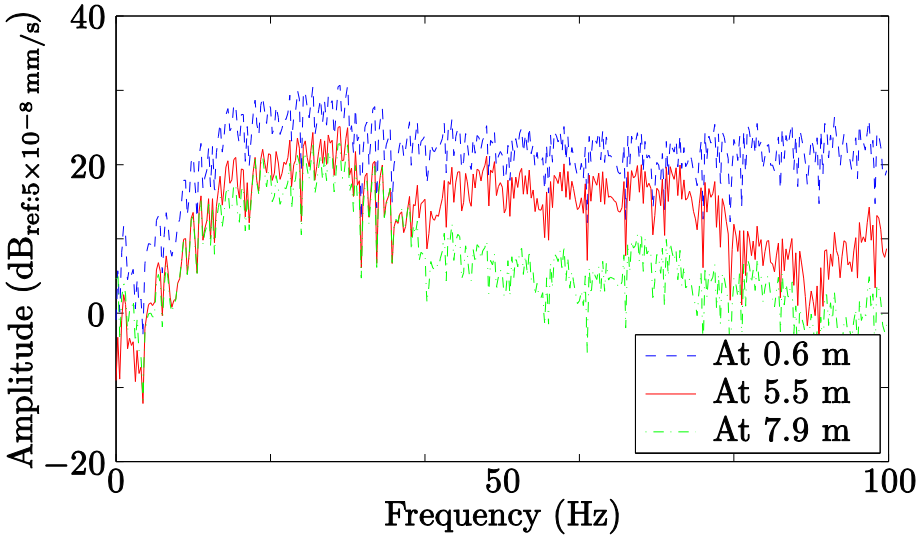


**Fig. 13 Frequency content of vibration velocities predicted at various distances from the track (site 12) for a tram T2006 running at 30 km/h on a rail joint (height 1 mm; length 5 mm)**

Figure 15 shows the peak particle velocities at the building locations as a function of defect size, considering a step-up and a step-down joint. The site 7 was studied for a T2006 tram running at a constant speed of 50 km/h. It appears that the non-linear effects at the wheel/rail contact are evident since the two step-type defects (same wheel/rail contact definition, see Figure 4) induce different ground vibration levels. This effect was also discussed by (Kouroussis et al., 2015b), where it was shown that vehicle/track dynamics have a strong influence on the vibration levels for such cases.

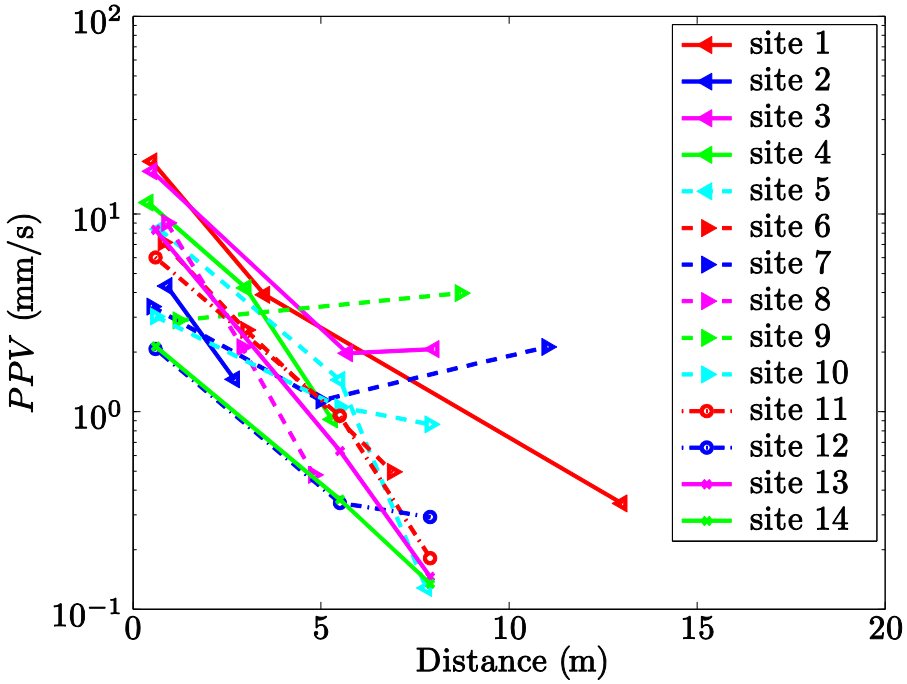


**Fig. 14 Predicted *PPV* as a function of all the studied sites for a tram T2006 running at 30 km/h on a pulse joint defect (height 1 mm; length 5 mm)**

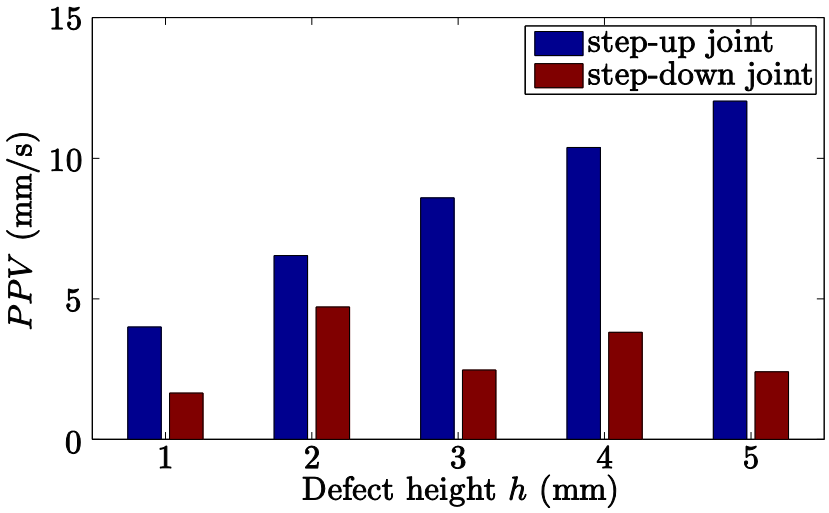


**Fig. 15 Predicted *PPV* as a function of the defect size for a tram T2006 running at 50 km/h on a step-up joint or on a step-down joint (variable height)**

Figure 16 shows the normalised peak particle velocities (*nPPV*) at the building locations as a function of the studied site and the tram speed $v$. The normalised *nPPV* is obtained by dividing each level by *PPV* value related to the reference speed of 20 km/h. This allows a more efficient comparison by semi-removing the effect of the layered soil and track-building distance to describe the overall relationship with train speed. Each site was studied for a constant tram speed (in the speed range 20–80 km/h). It appears that the general tendency is that *nPPV* level increases with vehicle speed and can be magnified by site type. A curve fitting, of type

$$nPPV \propto v_0^n \tag{11}$$

where $n$ is a power law constant, was added to the points to verify the correlation with increasing speed $v_0$. Some sites (ballasted track systems) presented elevated vibrations with increasing speed,

namely site 3 with $n = 2.3$ and sites 1 and 2 ($n = 1.6$), compared to the other sites ($n = 0.9$). This shows the influence of track systems on the vibration generated for increasing speed.

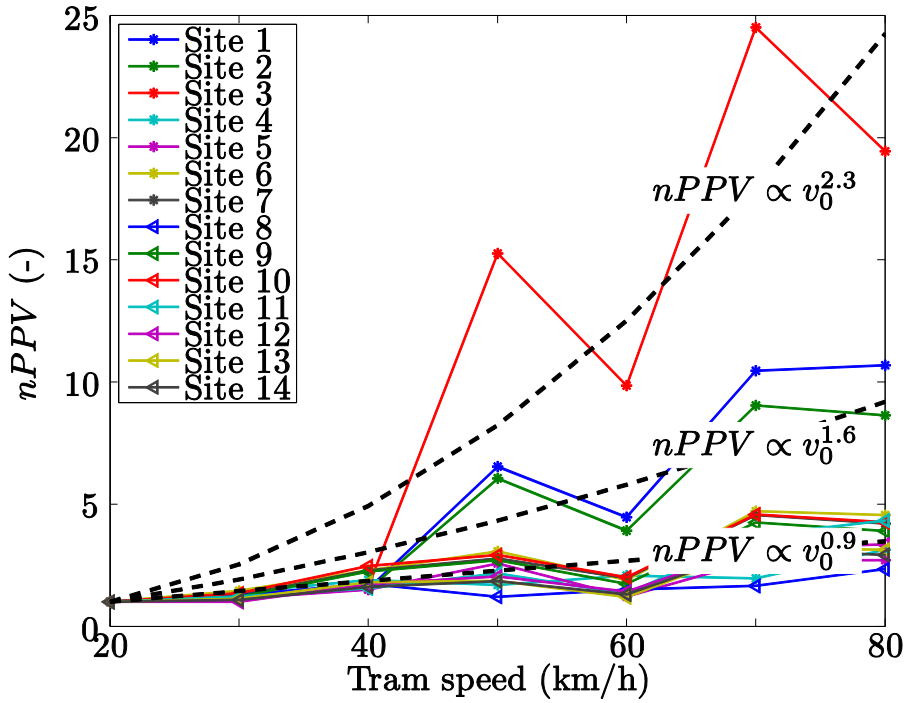


**Fig. 16 Predicted normalised *nPPV* as a function of speed for a tram T2006 running on a step-up joint (height 1mm) and for all the studied sites**

## 8. Conclusions

This paper presented a methodology to predict railway-induced ground vibrations in the presence of singular defects. These vibrations are due to the large forces generated between wheel and rail at the location of a defect. At the early stages of a vibration assessment, it is reasonable to consider that the effect of the vehicle influences the area close to the defect. Further, this research shows that source mobility functions are a useful tool to assess vibration control problems relating to light rapid transit system operations. Also, it presents an interesting alternative to the FRA2012 method as it is well suited to study locasized defects and provides ground vibration results in the time domain. Compared to pure numerical prediction methods, it offers a rapid way to evaluate vibrations with a minimum of amount of time required on site (only one single mobitity transfer function is sufficient at the location of interest).

## References


Auersch, L. (2015) "Realistic axle-load spectra from ground vibrations measured near railway lines." *International Journal of Rail Transportation*, 3(4), 180–200, doi: 10.1080/23248378.2015.1076624.

Bovey, E. C. (1983). "Development of an impact method to determine the vibration transfer characteristics of railway installations." *Journal of Sound and Vibration*, 87(2): 357–370. doi: 10.1016/0022-460X(83)90575-8.

Connolly, D. P., Kouroussis, G., Giannopoulos, A., Verlinden, O., Woodward, P. K. and Forde, M. C. (2014). "Assessment of railway vibrations using an efficient scoping model." *Soil Dynamics and Earthquake Engi*neering, 58: 37–47. doi: 10.1016/j.soildyn.2013.12.003.

Connolly, D. P., Kouroussis, G., Woodward, P. K., Verlinden, O., Giannopoulos, A. and Forde, M. C.

(2014). “Scoping prediction of re-radiated ground-borne noise and vibration near high speed rail lines with variable soils.” *Soil Dynamics and Earthquake Engineering*, 66: 78–88. doi: 10.1016/j.soildyn.2014.06.021.

Connolly, D. P., Marecki, G., Kouroussis, G., Thalassinakis, I. and Woodward, P. K. (2016). “The growth of railway ground vibration problems — a review.” *Science of the Total Environment*, 568: 1276–1282. doi: 10.1016/j.scitotenv.2015.09.101.

Federal Railroad Administration of the U.S. Department of Transportation (2012). *High-speed ground transportation. Noise and vibration impact assessment.* Technical Report DOT/FRA/ORD-12/15, Office of Railroad Development Washington.

Kouroussis, G., Connolly, D. P., Alexandrou, G. and Vogiatzis, K. (2015a). “The effect of railway local irregularities on ground vibration.” *Transportation Research — Part D: Transport and Environment*, 39: 17–30. doi: 10.1016/j.trd.2015.06.001.

Kouroussis, G., Connolly, D. P., Alexandrou, G. and Vogiatzis, K. (2015b). “Railway ground vibrations induced by wheel and rail singular defects.” *Vehicle System Dynamics*, 53(10): 1500–1519. doi: 10.1080/00423114.2015. 1062116.

Kouroussis, G., Gazetas, G., Anastasopoulos, I., Conti, C. and Verlinden, O. (2011). “Discrete modelling of vertical track–soil coupling for vehicle–track dynamics.” *Soil Dynamics and Earthquake Engineering*, 31(12): 1711–1723. doi: 10.1016/j.soildyn.2011.07.007.

Kouroussis, G., Van Parys, L., Conti, C. and Verlinden, O. (2013) “Prediction of ground vibrations induced by urban railway traffic: an analysis of the coupling assumptions between vehicle, track, soil, and buildings.” I*nternational Journal of Acoustics and Vibration*, 18(4): 163-172. doi: 10.20855/ijav.2013.18.4330

Kouroussis, G., Connolly, D. and Verlinden, O. (2014) “Railway-induced ground vibrations – a review of vehicle effects.” *International Journal of Rail Transportation*, 2(2): 69–110. doi: 10.1080/23248378.2014.897791.

Kouroussis, G. and Verlinden, O. (2015). “Prediction of railway ground vibrations: accuracy of a coupled lumped mass model for representing the track/soil interaction.” Soil *Dynamics and Earthquake Engin*eering, 69: 220–226. doi: 10.1016/j.soildyn.2014.11.007.

Nelson, J. T. and Saurenman, H. J. (1987). “A prediction procedure for rail transportation groundborne noise and vibration.” *Transportation Research Record*, 1143: 26–35.

Nielsen, J., Mirza, A., Cervello, S., Huber, P., Müller, R., Nelain, B. and Ruest, P. (2015). “Reducing train-induced ground-borne vibration by vehicle design and maintenance.” *International Journal of Rail Transportation*, 3(1): 17–39. doi: 10.1080/23248378.2014. 994260

Olivier, B., Connolly, D. P., Costa, P. A. and Kouroussis, G. (2016). “The effect of embankment on high speed rail ground vibrations.” *International Journal of Rail Transportation*, 4(4): 229–246. doi: 10.1080/23248378.2016.1220844.

Paneiro, G., Durão, F. O., Costa e Silva, M. and Falcão Neves P. (2016), “Artificial neural network model for ground vibration amplitudes prediction due to light railway traffic in urban areas.” *Neural Computing and Applications*, in press. doi: 10.1007/s00521-016-2625-9.

Talbot, J. P. (2014). “Lift-over crossings as a solution to tram-generated ground-borne vibration and re-radiated noise.” *Journal of Rail and Rapid Transit*, 228(8): 878–886. doi: 10.1177/0954409713499015.

Talbot, J. P. (2016). “Base-isolated buildings: towards performance-based design.” *Proceedings of the Institution of Civil Engineers — Structures and Buildings*, 169(8): 574–582. doi: 10.1680/jstbu.15.00057.

Verbraken, H., Lombaert, G. and Degrande, G. (2011). “Verification of an empirical prediction method for railway induced vibrations by means of numerical simulations.” *Journal of Sound and Vibration*, 330(8): 1692–1703. doi: 10.1016/j.jsv.2010.10.026.

Verlinden, O., Ben Fekih, L. and Kouroussis, G. (2013). “Symbolic generation of the kinematics of multibody systems in EasyDyn from MuPAD to Xcas/Giac.” *Theoretical & Applied Mechanics Letters*, 3(1): 013012. doi: 10.1063/2.1301 3012.

Vogiatzis, K. and Kouroussis, G. (2015). “Prediction and efficient control of vibration mitigation using

floating slabs: Practical application at Athens metro lines 2 and 3." *International Journal of Rail Transportation*, 3(4):, 215–223. doi: 10.1080/23248378.2015.1076622.

Zhai, W. and Sun, X. (1994). "A detailed model for investigating vertical interaction between railway vehicle and track." *Vehicle System Dynamics*, 23 (supplement): 603–615. doi: 10.1080/00423119308969544.

Zhu, S., Yang, J., Cai, C., Pan, Z. and Zhai, W. (2017). "Application of dynamic vibration absorbers in designing a vibration isolation track at low-frequency domain." *Journal of Rail and Rapid Transit*, 231(5): 546–557. doi: 10.1177/0954409716671549.

Zhu, S., Wang, J., Cai, C., Wang, K., Zhai, W., Yang, J. and Yan, H. (2017). "Development of a Vibration Attenuation Track at Low Frequencies for Urban Rail Transit." *Computer-Aided Civil and Infrastructure Engineering*, 32(9): 713–726. doi:10.1111/mice.12285.